Article

Super-resolution microscopy reveals nanoscale architecture and regulation of podosome clusters in primary macrophages

Podosome 3D Architecture

Microtubule
F-actin   Arp2/3
Cap proteins   Integrin
Paxillin   Myosin

Actin Paxillin

Actin Myosin IIA

Fen Hu, Donglan Zhu, Hao Dong, ..., Ke Xu, Leiting Pan, Jingjun Xu

plt@nankai.edu.cn

Highlights

3D-STORM delineates a snowman-like portrait of macrophage podosome core

3D-STORM maps the nanoscale arrangement of podosome ring components

Microtubules pass through podosomes at the layer of myosin and stabilize them

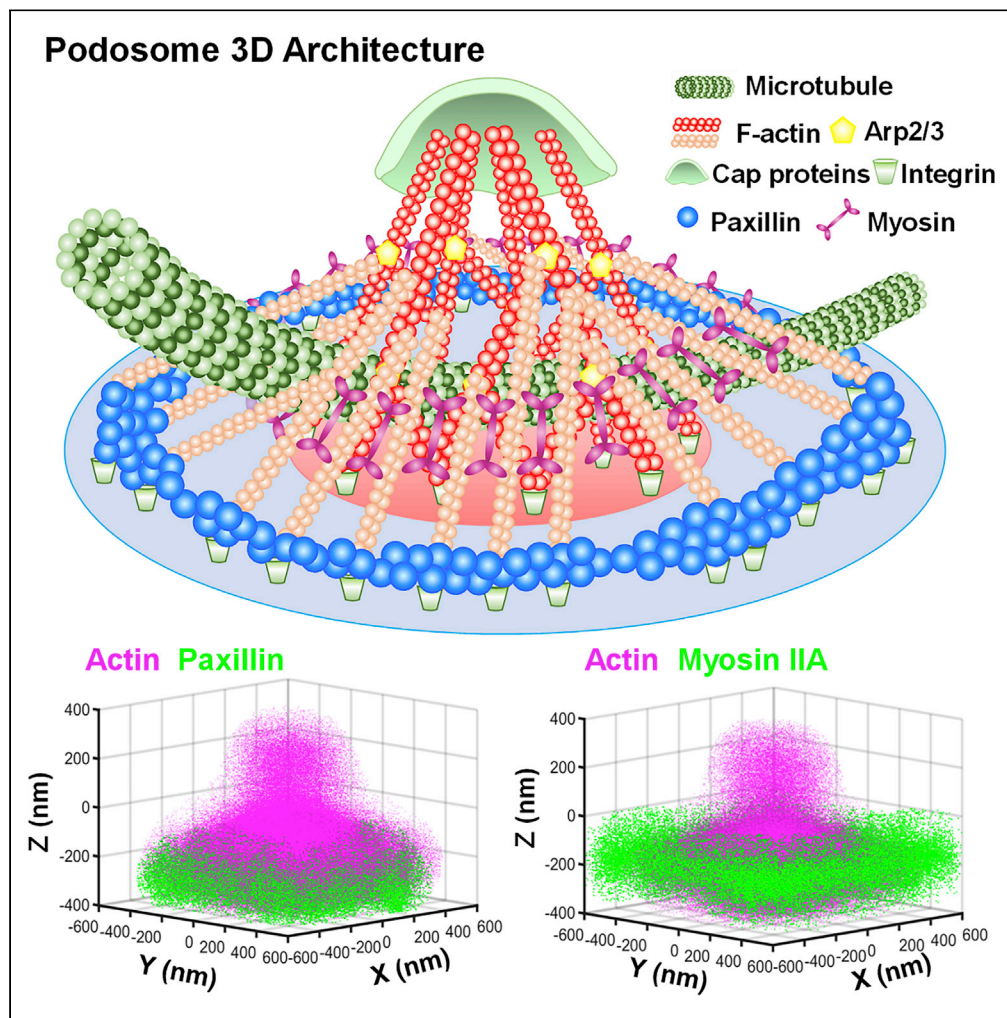Macrophage matrix degradation depends on the formation of podosome clusters

Article

Super-resolution microscopy reveals nanoscale architecture and regulation of podosome clusters in primary macrophages

Fen Hu,[1] Donglan Zhu,[1] Hao Dong,[1] Ping Zhang,[1] Fulin Xing,[1] Wan Li,[2] Rui Yan,[2] Jun Zhou,[3] Ke Xu,[2] Leiting Pan,[1,3,4,5,*] and Jingjun Xu[1,4]

SUMMARY

Podosomes, an important actin-based adhesive architecture, play critical roles in cell migration and matrix invasiveness. Here, we elucidate the ultrastructural organization and regulation of podosome clusters in primary macrophages. With three-dimensional stochastic optical reconstruction microscopy (3D-STORM), we achieve ~20/50 nm (lateral/axial) spatial resolution to resolve the mutual localization of podosome core and ring components, and further show that microtubules pass through podosomes at the layer of myosin IIA. The microtubule disruption-caused podosome dissolution is previously ascribed to Rho/ROCK-myosin signaling, yet inhibiting this pathway with Y27632 or blebbistatin only partially recovers podosome assembly, thus suggesting the contribution of the physical supporting of microtubules in stabilizing podosome structures. Through improved substrate-coating technique, we further corroborate that the matrix-degrading capability of macrophages depends on the formation of podosome clusters. Together, 3D-STORM super-resolution microscopy reveals the nanoscale spatial arrangement and the microtubule-dependent regulation of the matrix-degrading podosome clusters in macrophages.

INTRODUCTION

Macrophages are important regulators of the immune system, playing pivotal roles in tissue homeostasis.[1] They predominantly participate in innate and adaptive immunity by phagocytosis of the pathogen and antigen presentation.[2] They are also involved in inflammatory responses through the production of various cytokines.[3] The chemotaxis of macrophages into tissues is an essential step in the host response to infection or injury.[4,5] Although the extracellular matrix creates steric barriers to cell migration, macrophages can go through most body tissues through the continuous remodeling of intracellular cytoskeletons.[6] To date, several actin-based cytoskeletal adhesive and invasive structures, mainly involving focal adhesions and podosomes, have been reported to drive the migration process of macrophages.[7,8]

Macrophages constitutively form numerous podosomes with distinct structural, functional, and dynamic characteristics.[9,10] Podosome is a multimolecular assembly with a protrusive actin core module and an adhesive ring module composed of integrin and cytoskeletal adaptor proteins, including paxillin, talin, and vinculin.[11] In recent years, the third cap module of this characteristic structure has been successively determined.[12–14] In different cell types, individual podosomes are arranged into higher ordered superstructures, including diversely shaped clusters in macrophages and dendritic cells,[9,10,15] ring-shaped "rosettes" in endothelial cells,[16] and circular belts in osteoclasts.[17] Podosomes are specialized cell-matrix contacts with an inherent ability to degrade extracellular matrix (ECM), thus facilitating cell migration in the tissue microenvironment.[18,19] Besides, they can act as sensors for substrate topography by actively probing the rigidity of ECM.[15,20,21] Loss of podosome components may lead to dysfunction of macrophages or podosome-related diseases such as Wiskott-Aldrich syndrome and Frank-Ter Haar Syndrome.[22,23]

As a highly dynamic structure, podosome undergoes a series of processes, including initiation, assembly, maturation, and turnover.[24] Its assembly and disassembly are regulated by a variety of intracellular signaling pathways and factors.[25,26] Recent advances in microscopic and analytical techniques offer new

opportunities to resolve the ultrastructure, organization, and dynamics of podosomes at the nano-scale.[27–35] For instance, using dual-color stochastic optical reconstruction microscopy (STORM)[28] and three-dimensional (3D)-SIM,[30,33] it has been revealed that podosome cores are interconnected and linked to the ventral membrane by radiating actin filaments to drive mesoscale podosome organization in dendritic cells. With structured illumination super-resolution microscopy (SIM) and stimulated emission depletion microscopy, Walde et al. describe a distinctly polygonal shape rather than a round shape as previously assumed for vinculin within the podosome ring in macrophages.[29] Using DONALD, a 3D nanoscopy technique with 20 nm isotropic localization precision, Bouissou et al. unveil the vertical extension of talin in the podosome ring in macrophages, indicating that the ring sustains mechanical tension.[31] Moreover, Joosten et al. perform super-resolution correlative light and electron microscopy to study the organization of multiple proteins at the ventral plasma membrane of dendritic cells, and elucidate a differential organization of vinculin and zyxin with respect to the actin filaments at podosomes.[32]

In the present work, we focus on the ultrastructural spatiotemporal organization and regulation of podosomes formed in primary mouse peritoneal macrophages, as well as their matrix degradation function. Utilizing 3D-STORM super-resolution microscopy,[36–38] we visualize the nanoscale 3D landscape of individual macrophage podosomes with ∼20/50 nm (lateral/axial) spatial resolution. Through a particle superimposing method, we provide the precise mutual localization of podosome actin core and ring component proteins. Moreover, we reveal the physical coupling between podosome and microtubule cytoskeletons at the layer of myosin IIA, and suggest the involvement of microtubule interactions in maintaining podosome integrity. With an improved matrix-coating technique derived from photolithography, we show good correlations between the capability of the macrophage to form podosome clusters and matrix degradation. Finally, we demonstrate that the modulation of actomyosin and microtubule cytoskeletons significantly influences the podosome-based matrix degradation by macrophages.

RESULTS

The ultrastructural organization of podosomes in primary macrophages and corresponding extracellular matrix degradation

Primary peritoneal macrophages were isolated from C57BL/6 mice and cultured in RPMI1640 medium supplemented with 10% FBS following standard tissue-culture protocols. To explore the spatiotemporal architectural arrangement of podosomes in macrophages at the nanoscale level, we fixed the cells at different *in vitro* culture timepoints for fluorescence labeling of F-actin or paxillin, and performed 3D-STORM microscopy to achieve ∼20/50 nm (lateral/axial) spatial resolution optically.[36–38] As shown, representative STORM images of actin/paxillin for macrophages after 4 and 18 h culture demonstrated substantially improved lateral and axial resolutions than the conventional, diffraction-limited images (Figures 1A, 1B and S1). Macrophages could form puncta-like adhesion structures as early as cultured for 4 h (Figure 1A). With extended culturing, these puncta-like structures matured and appeared as typical podosomes (Figure 1B). From the 3D-STORM images of single podosomes, it was thus clearly shown that F-actin localized to a snowman-shaped region at the podosome core (Figures 1A and 1B). Individual podosomes interconnected by a network of actin filaments usually gathered together to form large clusters in local regions in the 18 h cells (Figure 1B). Quantification of the STORM images showed that the F-actin cores of podosomes in macrophages were nearly circular (with ∼80% podosomes having circularity >0.7) (Figure 1C), and the average radius of the podosome F-actin core was ∼390 nm (Figure 1D). Podosome clusters are defined as groupings of more than ten individual podosomes in a restricted area (>16 μm^2) of the cell (such as the regions surrounded by the yellow curves in Figure S2). The average area of podosome clusters was 80 μm^2 (Figure S2), and the density of the podosomes in the clusters was ∼0.66/μm^2 (Figure 1E).

To facilitate the quantitative analysis of the matrix degradation by macrophages, we developed a new substrate-coating technique derived from photolithography. Specifically, the evaporation of a layer of hexamethyldisilazane on the glass surface (Figure S3A) significantly enhanced the homogeneous adhesion of fibronectin (FN) than simply coating FN on the untreated glass surface (Figure S3B) or on the poly-L-lysine)coated glass surface (Figure S3C). With the improved matrix coating, we followed how the macrophages gradually initiated extracellular matrix degradation through the loss of fluorescently labeled FN (Figures 1F and S4). The positions of FN degradation colocalized substantially with the podosome clusters (Figure S4). Statistics indicated that the percentages of podosome cluster-positive macrophages increased with culture time, which were 3.1 ± 5.4%, 19.6 ± 9.5%, 31.4 ± 10.6%, and
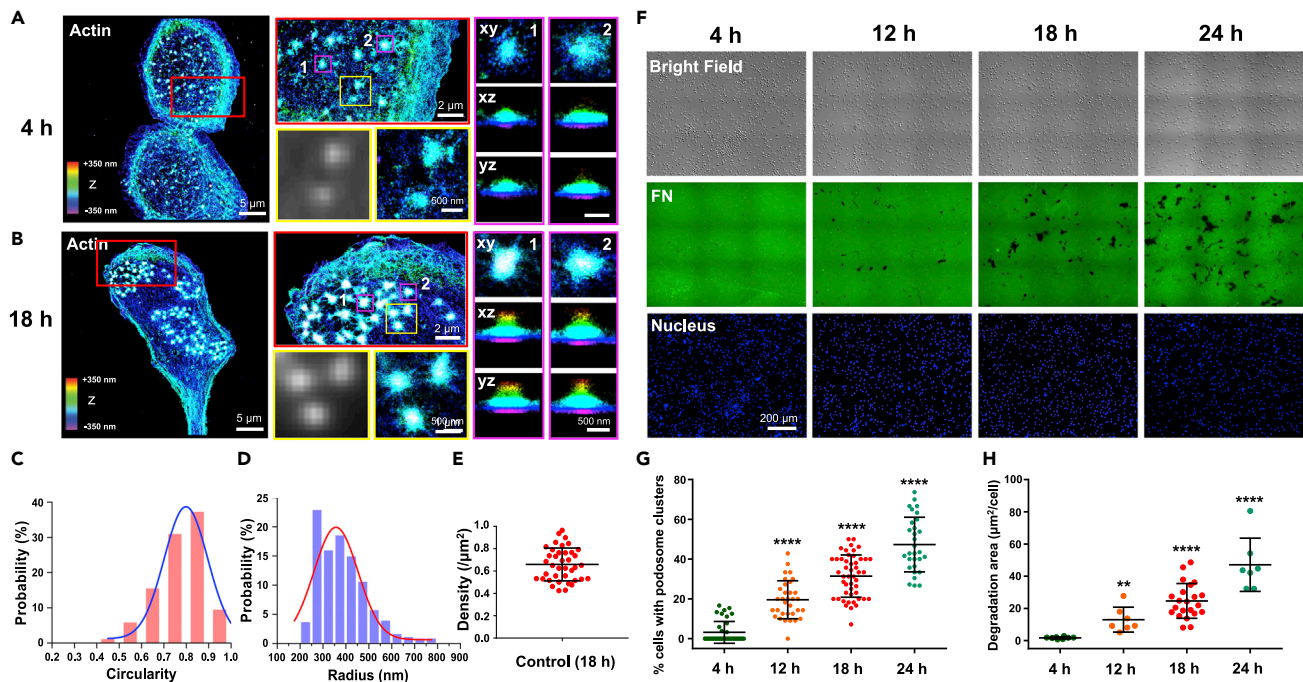
Figure 1. The formation of podosome clusters and degradation of extracellular matrix in mouse peritoneal macrophage with different culture time

(A and B) Representative 3D-STORM images of actin in individual mouse peritoneal macrophages after culturing for 4 (A) and 18 h (B). The z-positions are color-coded according to the color bar: Violet indicates positions closest to the substratum and red indicates farthest. The red boxes are selected regions, and their corresponding zoom-in images are shown on the right. The yellow boxes are selected regions from the red boxes containing several podosomes, and the zoom-in images compared to the diffraction-limited epifluorescence images of the same regions are shown below. Besides, the profiles of actin in the xz and yz plane in two individual podosomes (magenta box) are shown on the right.

(C–E) Summary of the circularity (C) and radius (D) of the podosome actin core (n = 378), as well as the density (E) of podosome clusters in macrophages cultured for 18 h. The density of a podosome cluster = The number of podosomes in a cluster/The area of this podosome cluster.

(F) Representative images showing the FN degradation by macrophages after culturing for 4, 12, 18, and 24 h. The first line shows images of macrophages in bright field (combination of nine adjacent fields of view captured by a 10× objective into an enlarged field of view). The second line shows images of fluorescently labeled FN at the same field of vision. The third line shows images of cell nuclei stained by DAPI.

(G) Box chart showing a summary of the percentage of cells with podosome clusters at the indicated time points. Each data point indicates the percentage of cells with podosome clusters in each of the images captured by a 40× objective. The podosome cluster-positive cells were counted manually by determining if the cell contained groupings of >10 individual podosomes in a restricted area, or if the area occupied by grouping podosomes in the cell was >16 μm^2 (the average area occupied by one podosome was 1.6 μm^2).

(H) Box chart showing a summary of the degradation area per cell at the indicated time points. Each data point indicates the degradation area per cell in each image of the big field of vision. Values are reported as means ± SD from at least three independent experiments. Statistics were performed by unpaired Student's t test. Asterisks indicate statistical significance comparing with 4 h group. *p < 0.05, **p < 0.01, ***p < 0.001, ****p < 0.0001, ns, not significant (p > 0.05).

47.3 ± 13.7% after incubating for 4, 12, 18, and 24 h, respectively (Figure 1G). Meanwhile, the matrix degradation activity by macrophages (expressed by degradation area per cell, Figure S5) was also dependent on the culture time course, which was 1.7 ± 0.6 μm^2/cell, 13.0 ± 7.7 μm^2/cell, 24.7 ± 10.8 μm^2/cell, and 47.1 ± 16.5 μm^2/cell after culturing for 4, 12, 18, and 24 h, respectively (Figure 1H). With live-cell imaging, we further found that the macrophages degraded the matrix in a "plaque erasing" manner (Figure S6 and Video S1). These data together indicated that the formation of cluster-shaped podosome superstructures in the cultured macrophages initiated strong matrix degradation in a time-dependent manner.

Dual-color 3D-STORM reveals the nanoscale mutual localization of the F-actin core, paxillin ring, and myosin IIA ring in the macrophage podosomes

To study the spatial arrangement of the podosome components in greater detail, we performed dual-color 3D-STORM microscopy for macrophages after 18 h culturing. Dual-color STORM image of F-actin and paxillin verified the unique "core + ring" ultrastructure for each podosome (Figures 2A–2D), as extensively described in previous documents.[9–11] 3D-STORM images of single podosomes showed that paxillin
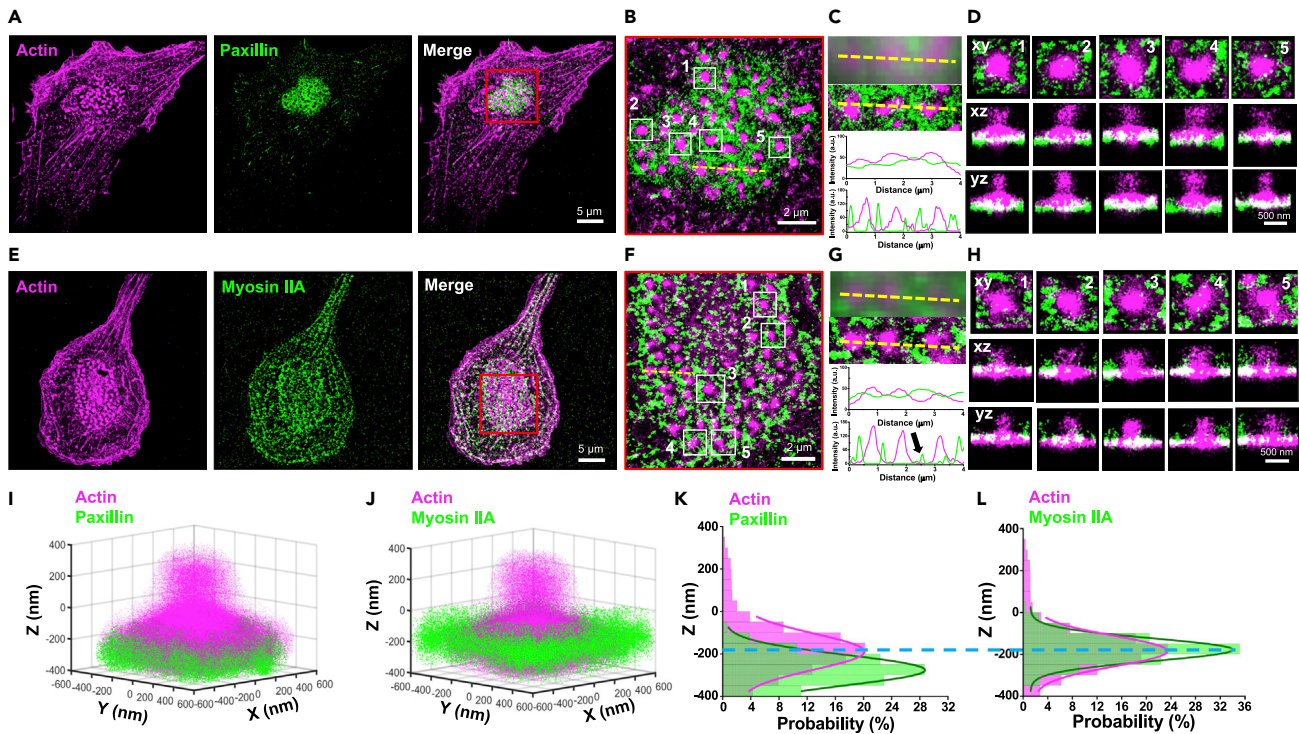
Figure 2. The spatial relationship between the F-actin core, paxillin ring, and myosin IIA ring in podosomes of macrophages revealed by two-color 3D-STORM

(A and E) Representative two-color STORM results of actin/paxillin (A) and actin/myosin IIA (E) in individual macrophages cultured for 18 h. A separate image of the actin (magenta) and paxillin/myosin IIA (green), and overlaid image are shown, respectively.

(B and F) Zoom-in overlaid image of a selected region (red box) in (a) and (b). The white boxes are selected regions containing individual podosomes.

(C and G) Magnified views of three podosomes passing through by the yellow dotted line in (B) and (F) compared with the corresponding diffraction-limited epifluorescence images. Besides, the profiles of actin/paxillin (C) and actin/myosin IIA (G) intensity taken along the yellow dotted lines are show down.

(D and H) The profiles of actin and paxillin/myosin IIA in the xz and yz plane in five individual podosomes from (B) and (F) (white boxes).

(I and J) Three-dimensional composite graphics showing the spatial topography of actin/paxillin (I) and actin/myosin IIA (J) in podosome structure by the particle superimposing method.

(K and L) The distribution profiles of z-positions for actin/paxillin (K) and actin/myosin IIA (L) by projection of the composite graphics in z direction.

localized on the ring surrounding the F-actin core at the ventral plasma membrane layer (Figure 2D). We further resolved the spatial relationship between the podosome F-actin core and non-muscle myosin IIA by dual-color 3D-STORM. Myosin IIA is known to be excluded from the Arp2/3 complex-generated branched F-actin core while crosslinking the unbranched actin filaments radiating from the core or inter-connecting adjacent podosomes[18,30,33]; thereby, it can be present both in the podosome ring structure and connecting cables. From the dual-color 3D-STORM images, we clearly visualized that myosin IIA also localized to the macrophage podosomes (Figures 2E–2H). Interestingly, whereas in-plane projections of the 3D-STORM images showed that myosin IIA surrounded the core structure similarly as paxillin (Figures 2E–2H), vertical projections indicated that the myosin IIA rings positioned in a focal plane slightly above the paxillin rings (Figures 2D and 2H).

Although 3D-STORM microscopy greatly improves the lateral and axial spatial resolutions when compared to the conventional fluorescence microscopy (Figures 2C and 2G), signal loss in the dual-color STORM image of single podosomes is still inevitable, especially for the ring proteins due to incomplete labeling (Figures 2D and 2H, and the black arrow in Figure 2G showed occasional weak signal for myosin IIA ring). Accordingly, we developed a particle superimposing routine that allowed us to combine the information from multiple images of single podosomes. After identifying the xy-center of each actin core, the signal particles in sixty individual podosomes were aligned and summed following the recognized actin centers to generate composite 3D graphics of different podosome component pairs (actin/paxillin and actin/myosin IIA) (Figures 2I and 2J). These 3D graphics clearly and visually exhibited a snowman-like portrait of the

podosome actin core, as well as the paxillin or myosin IIA ring structures around the F-actin core. From the derived z-distribution profiles of actin/paxillin (Figure 2K) and actin/myosin IIA (Figure 2L), it was found that the peak z position of paxillin signal particles was ∼90 nm lower than that of actin by Gaussian fitting (Figure 2K), whereas the peak z position of myosin IIA was almost coincided with that of actin (Figure 2L). Therefore, podosome-localized myosin IIA distributed in a focal plane ∼90 nm higher than paxillin. Together, through the combination of 3D-STORM with particle superimposing, we unveiled the precise spatial relationship of the F-actin core, paxillin ring, and myosin IIA ring in macrophage podosomes at the nanoscale level.

3D-STORM reveals microtubules pass through podosomes at the layer of myosin IIA in macrophages

Besides close interconnections with the intracellular actomyosin network, podosomes have also been reported to have direct or indirect linkage to the microtubule cytoskeletons.[39–41] However, the detailed information on how microtubules interact with podosomes remains elusive due to the diffraction limit of traditional microscopy. Here, dual-color 3D-STORM results of actin and α-tubulin showed that in some cases, microtubules could pass through podosomes at z positions above the ventral membrane layer in macrophages (Figure 3A). Similarly, we applied our particle superimposing method to obtain the composite z-distribution profile of microtubules that passed through podosomes. It showed that the z height of α-tubulin almost coincided with that of myosin IIA (Figure 3B right, also shown in Figure 2I), thus suggesting that the podosomes and microtubules may be coupled by myosin IIA (Figure 3C). Our dual-color 3D-STORM imaging of α-tubulin against paxillin and myosin IIA further showed that microtubules could pass through the paxillin/myosin IIA rings of podosomes, and α-tubulin localized above paxillin whereas overlapped with the typical height of myosin IIA (Figures 3D and 3E). Together, our results implicated a direct mechanical link between microtubules and podosomes at the layer of myosin IIA in primary macrophages, which may provide a physical support for maintaining the integrity of podosome structures.

Actomyosin cytoskeletons influence the formation and organization of podosome clusters in macrophages

We further investigated the roles of actomyosin machinery in the formation and organization of podosome clusters in macrophages. To this end, we cultured macrophages *in vitro* for 16 h, and then performed different pharmacological treatments for 2 h. The application of actin polymerization inhibitor cytochalasin D (Cyto D) resulted in a complete disruption of the actin network and disassembly of the podosome clusters in macrophages (Figures 4H, S7A, and S7D), indicating a crucial role of actin polymerization in the assembly and stability of podosomes. We next treated the cells with two drugs targeting myosin IIA: one is the myosin II ATPase blocker blebbistatin (Bleb); the other is the Rho-associated kinase (ROCK) antagonist Y27632, which inhibits the phosphorylation of the myosin light chain and thus also reduces the activity of myosin IIA. Both Bleb (Figures 4A, S7B, S8A, and S8B) and Y27632 (Figures 4B, S7C, S8A and S8C) clearly prevented the formation of actin stress fibers and myosin IIA filaments in macrophages. Notably, treatment with Bleb led to the dislocation of myosin IIA from the region of podosome clusters, thereby suppressed the presence of myosin IIA ring structures (Figures 4A, S8A, and S8B). Moreover, fewer microtubules were connected to the podosomes in the Bleb- or Y27632-treated cells comparing to the control group (Figure S9). However, the two inhibitors had little effect on the existence of the actin core (Figures 4A, 4B, S7B, and S7C) and paxillin ring (Figures S7E and S7F) of podosome clusters. Statistical results showed that the Bleb- and Y27632-treated group had 24.6 ± 11.7% and 28.7 ± 14.7% podosome cluster-positive cells, respectively, when the untreated control group had 32.8 ± 13.8% podosome cluster-positive cells (Figure 4H). Additionally, the circularity and radius of podosome actin core, as well as the area and density of podosome clusters were largely unchanged after treatment with Bleb and Y27632 (Figures 4C–4G and S2). Therefore, actin and myosin II differentially impacted the organization of podosome clusters formed in macrophages. The modulation of myosin IIA activity slightly suppressed the occurrence of podosome clusters but substantially influenced the delicate spatial orchestration of this superstructure.

Microtubules regulate the assembly of podosome clusters in macrophages not entirely via the Rho/ROCK-myosin IIA pathway

While the role of the actomyosin network in podosome formation and turnover is well established, the involvement of microtubule cytoskeletons is less well defined. In line with previous documents,[42] our results showed that treating macrophages with microtubule-depolymerizing drug nocodazole (Noc) (Figure S10A) led to the drastic disassembly of podosome clusters (Figures 5A, S10B, and S10C) that accompanied the
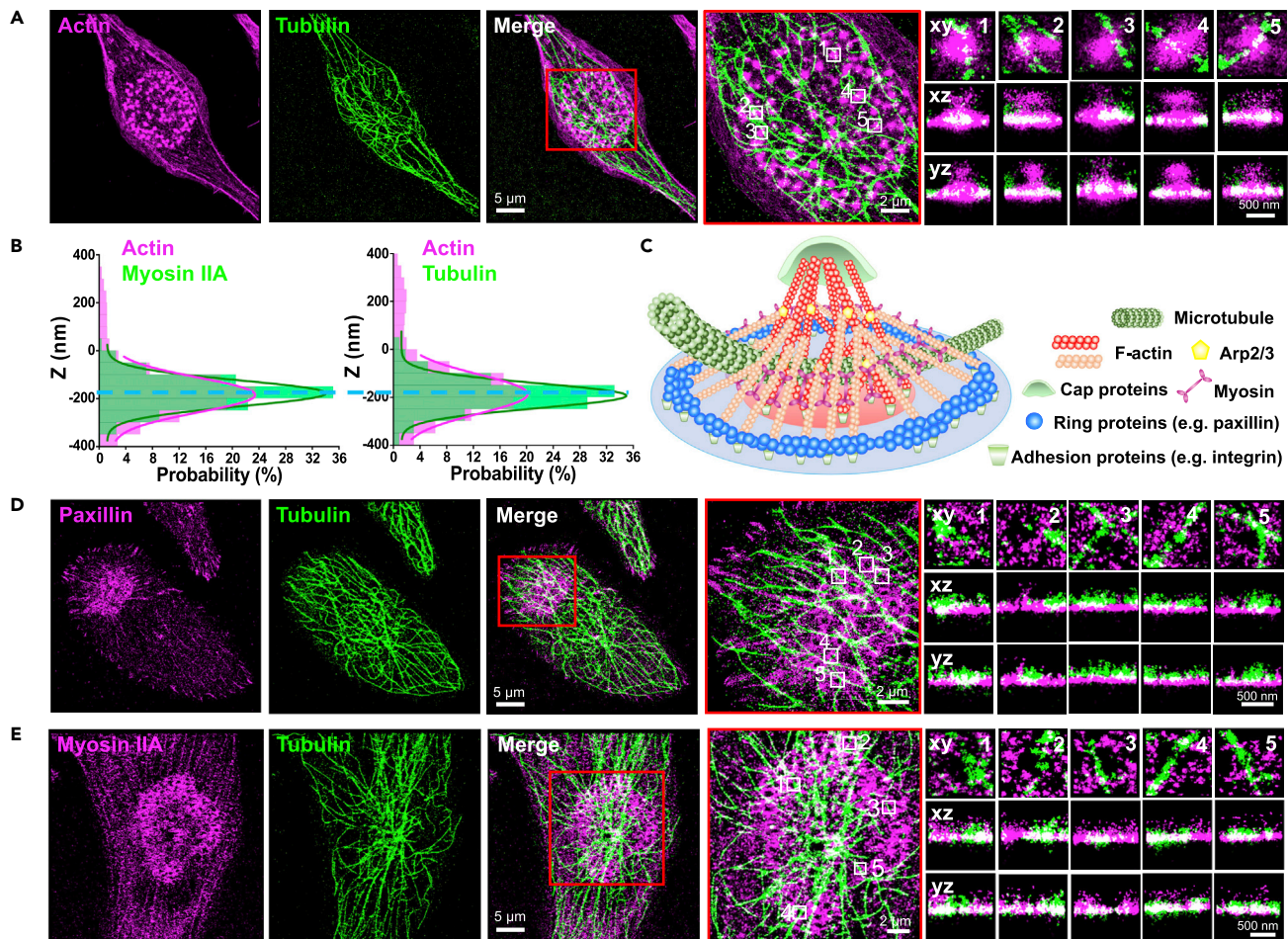
Figure 3. The crosslink between podosome and microtubules in macrophages revealed by two-color 3D-STORM

(A, D, and E) Representative two-color STORM results of α-tubulin with actin (A), paxillin (D), and myosin IIA (E) in individual macrophages cultured for 18 h. Separate images of the actin (magenta) and α-tubulin (green), the overlaid images, and the zoom-in images of a selected region (red box) are shown, respectively. The profiles of actin/α-tubulin (A), α-tubulin/paxillin (D), and α-tubulin/myosin IIA (E) in the xz and yz plane in five individual podosomes (white boxes) are shown on the right.

(B) Summary of the z positions of actin and α-tubulin in podosomes compared with that of actin and myosin IIA (already shown in Figure 2I) (n = 60 podosomes from 12 cells in three independent experiments).

(C) Three-dimensional ultrastructure model of a podosome depicting the spatial localization relationship of podosome components and microtubule connection. Podosomes are dome-like structures in macrophages. Arp2/3-branched actin filaments (red) compose the podosome core surrounded by unbranched actin filaments (orange) bundled by myosin IIA (purple). Cap proteins (green) are located on top. Actin filaments interact through ring proteins (e.g., blue: paxillin) to adhesion molecules (e.g., integrin) which are connected to the extracellular matrix. Microtubules (dark and light green) cross podosomes at the level of myosin IIA.

enhanced formation of actin stress fibers (Figure S11A), focal adhesions (Figure S11D), as well as myosin IIA filaments (Figures 5A and S10C). Comparing to the control group, the percentage of podosome cluster-positive cells under Noc treatment was reduced from 32.8 ± 13.8% to 4.2 ± 7.3% (Figure 5C). This result was previously ascribed to the increase in the Rho/ROCK-dependent actomyosin contractile activity.[42,43] However, we found that inhibiting the Rho/ROCK signaling by Y27632 only partially recovered the Noc-induced podosome disassembly (fraction of podosome cluster-positive cells: 4.2 ± 7.3% for Noc alone vs. 11.2 ± 7.9% for Noc + Y27632 vs. 32.8 ± 13.8% for control, Figure 5C). Meanwhile, Bleb, the blocker of myosin ATPase downstream of Rho/ROCK, did not induce the reemergence of podosome clusters at all (fraction of podosome cluster-positive cells: 4.6 ± 5.5% for Noc + Bleb vs. 4.2 ± 7.3% for Noc alone, Figure 5C). These results indicated that the microtubules disruption-caused podosomes dissolution in macrophages was not entirely accounted for by the commonly assumed Rho/ROCK-myosin IIA signaling.
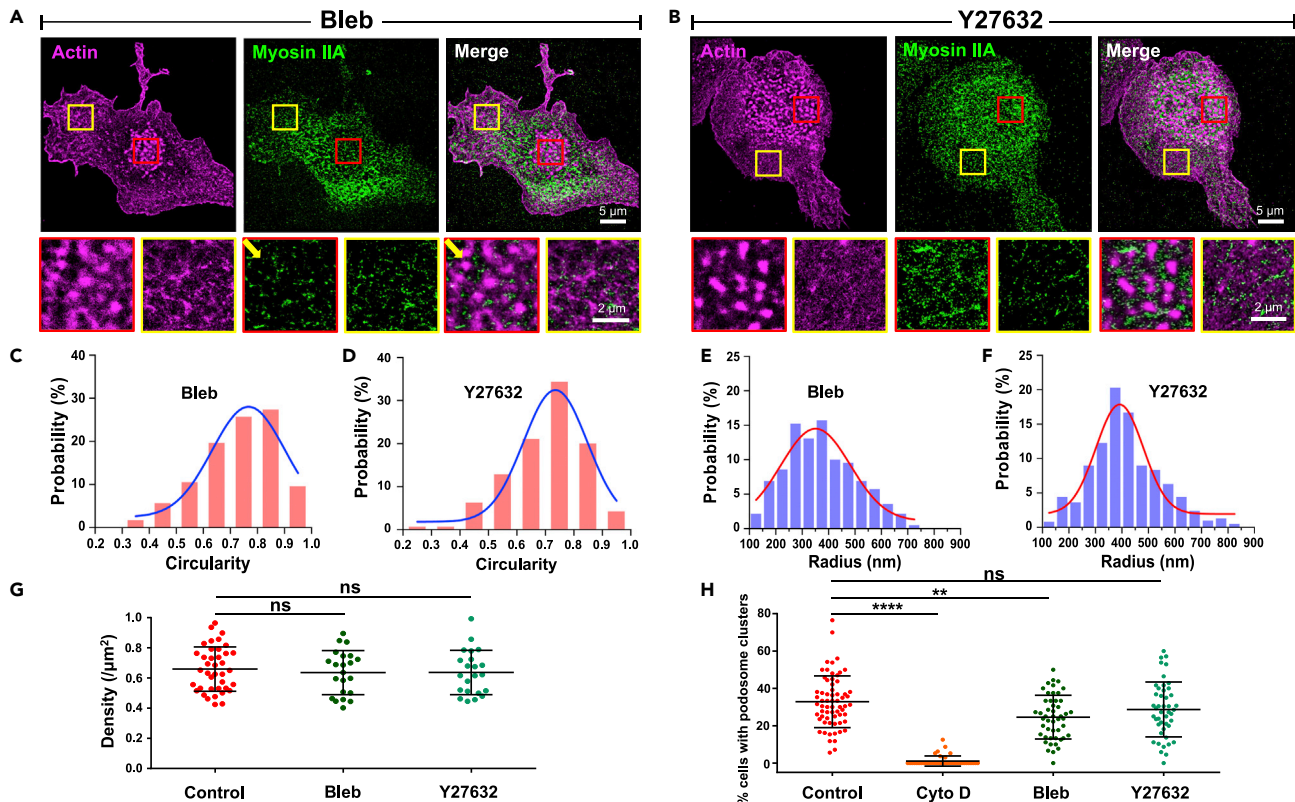
Figure 4. The effects of regulating myosin IIA activity on the organization of podosome clusters in macrophages

(A and B) Representative two-color STORM results of actin and myosin IIA in individual macrophages cultured for 16 h and then treated with Bleb (20 μM) or Y27632 (20 μM) for 2 h. Separate images of the actin (magenta) and myosin II (green), and overlaid images are shown above, respectively, and the zoom-in images of two selected regions (red and yellow box) are shown below. The yellow arrow showed myosin IIA dislocation from the region of podosome clusters induced by Bleb.

(C and D) Summary of the circularity of the podosome actin core in Bleb (n = 426) and Y27632 (n = 630) pretreated macrophages.

(E and F) Summary of the radius of the podosome actin core in Bleb (n = 426) and Y27632 (n = 630) group.

(G) Summary of density of podosome clusters in Bleb and Y27632 group.

(H) Box chart showing a summary of the percentage of cells with podosome clusters in macrophages cultured for 16 h and then treated with or without Cyto D (1 μM), Bleb (20 μM), or Y27632 (20 μM) for 2 h. Values were reported as means ± SD from at least three independent experiments. Statistical significances were analyzed by unpaired Student's t test. *p < 0.05, **p < 0.01, ***p < 0.001, ****p < 0.0001, ns, not significant (p > 0.05).

Interestingly, Noc in combination with Bleb led to the dislocation of myosin IIA from most areas of the cell for accumulation in the perinuclear area (Figures 5B and S12B), forming myosin IIA filaments that were detrimental to podosome assembly (Figure S12C). Similarly, Noc together with Y27632 retained partial formation of myosin IIA filaments in local regions of the cell (Figures 5A, 5B and S13). These data implicated crosstalk between myosin IIA and the microtubule cytoskeleton in the regulation of podosome formation and dissolution. According to our results, we suggested that microtubules could regulate the assembly dynamics of podosomes via two independent pathways: one is the Rho/ROCK-myosin IIA signaling (signal pathway) (Figure 5D right), and the other is the physical support through crossing podosomes at the layer of myosin IIA (physical pathway) (Figure 5D left).

The matrix degradation by podosome clusters in macrophages is also regulated by the intracellular actomyosin and microtubule cytoskeletons

Finally, we investigated the effects of actomyosin and microtubule cytoskeletons on the matrix degradation function of macrophages by using above inhibitors. In this series of experiments, we decreased the working concentration of the inhibitors in order to prevent the influence of long-term application with high-dose drugs on cell adherence and/or viability. Treatment with Cyto D (Figures 6B, 6I, and S14B) or Noc (Figures 6E, 6I, and S14E) for 18 h significantly inhibited the matrix degradation capability of macrophages compared with the control group (Figures 6A and S14A). Correspondingly, Cyto D and Noc also resulted in
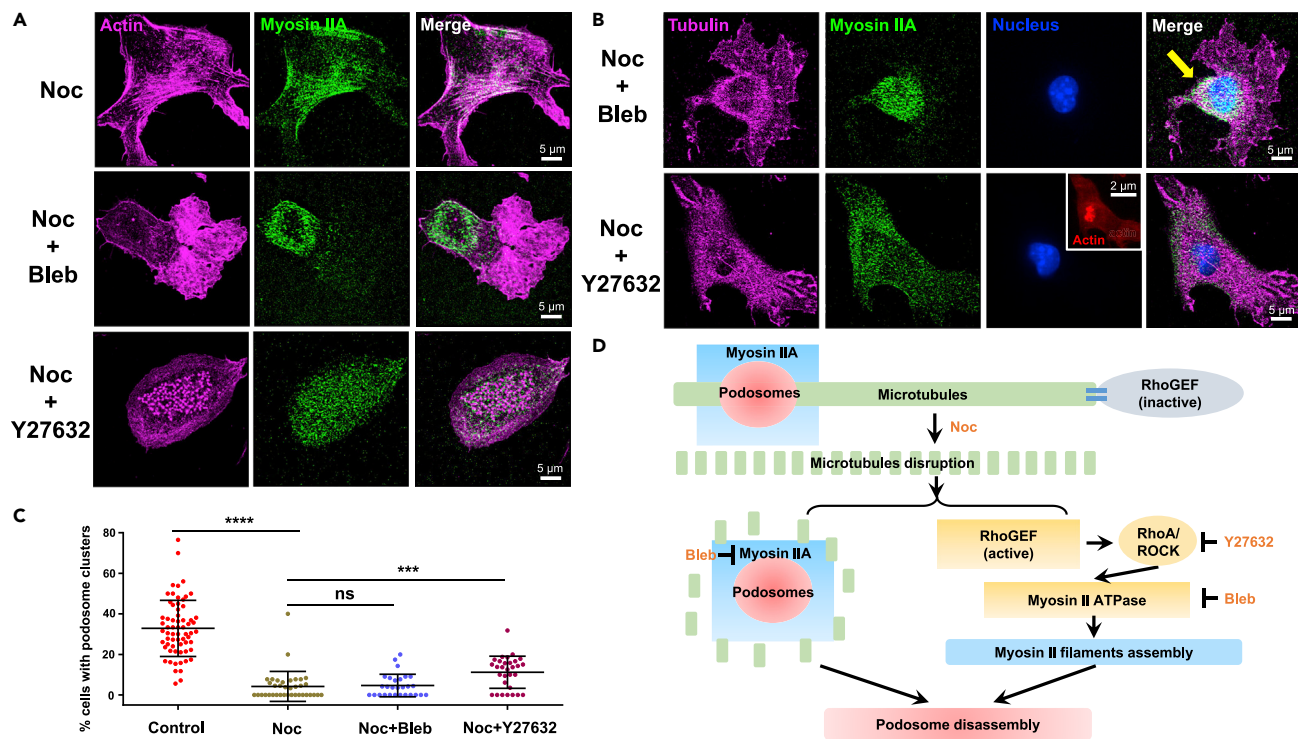
Figure 5. The effects of inhibiting Rho/ROCK-myosin IIA signaling on nocodazole-induced podosome clusters disassembly

(A) Representative two-color STORM results of actin and myosin IIA in individual macrophages cultured for 16 h and then treated with Noc (10 μM), Noc (10 μM)+Y27632 (20 μM), and Noc (10 μM)+Bleb (20 μM) for 2 h. Separate images of the actin (magenta) and myosin IIA (green), and overlaid image are shown, respectively.

(B) Representative two-color STORM results of α-tubulin and myosin IIA in individual macrophages cultured for 16 h and then treated with Noc (10 μM)+Y27632 (20 μM) and Noc (10 μM)+Bleb (20 μM) for 2 h. Separate images of the α-tubulin (magenta), myosin IIA (green), nucleus (blue), and overlaid image are shown, respectively. Y27632 partially recovered the podosome formation, thus typical images for Noc + Y27632-treated cells with podosome clusters are shown. The inserted epifluorescence image showed phalloidin Alexa Fluor 488-labeled actin (red) of the same region. The yellow arrow showed the accumulation of myosin IIA in the perinuclear area induced by Noc + Bleb.

(C) Box chart showing a summary of the percentage of cells with podosome clusters in macrophages cultured for 16 h and then treated with Noc (10 μM), Noc (10 μM)+Y27632 (20 μM), or Noc (10 μM)+Bleb (20 μM) for 2 h. Values are reported as means ± SD from at least three independent experiments. Statistical significances were analyzed by unpaired Student's t test. *p < 0.05, **p < 0.01, ***p < 0.001, ****p < 0.0001, ns, not significant (p > 0.05).

(D) Schematic diagram of the mechanisms on microtubules disruption-caused disassembly of podosomes in macrophages.

a dramatic decrease in the percentages of macrophages with podosome clusters (Figure 6H), similar to the results of drug treatment for 2 h (Figure 5C). The application of low concentration Bleb (Figures 6C and S14C) or Y27632 (Figures 6D and S14D) alone for 18 h only slightly reduced the percentages of macrophages with podosome clusters (Figure 6H) and the matrix degradation activity of macrophages (Figure 6I). Furthermore, we also explored the role of Rho/ROCK-myosin IIA signaling in Noc-induced loss of matrix degradation function. Consistent with our above results on podosome reassembly, Noc-induced inhibition in matrix degradation was only partially recovered by Bleb (Figures 6F, 6I, and S14F) and Y27632 (Figures 6G, 6I, and S14G). These results together demonstrate that both the actin and tubulin cytoskeletons play essential roles in regulating the podosome cluster-based matrix degradation function of macrophages.

DISCUSSION

Podosome is a dynamic adhesion architecture formed predominantly in cells of the myelomonocytic lineage, including macrophages, dendritic cells, osteoclasts, and microglia.[11] It plays key roles in cell adhesion, migration, fusion, mechanosensing, as well as extracellular matrix degradation.[18–21,44–46] In this work, we presented rich information on how podosomes are organized into cluster-like mesoscale superstructures in mouse peritoneal macrophages that initiate strong matrix degradation. Then, combining 3D-STORM super-resolution light microscopy with a particle superimposing method, we delineated the clear 3D portrait
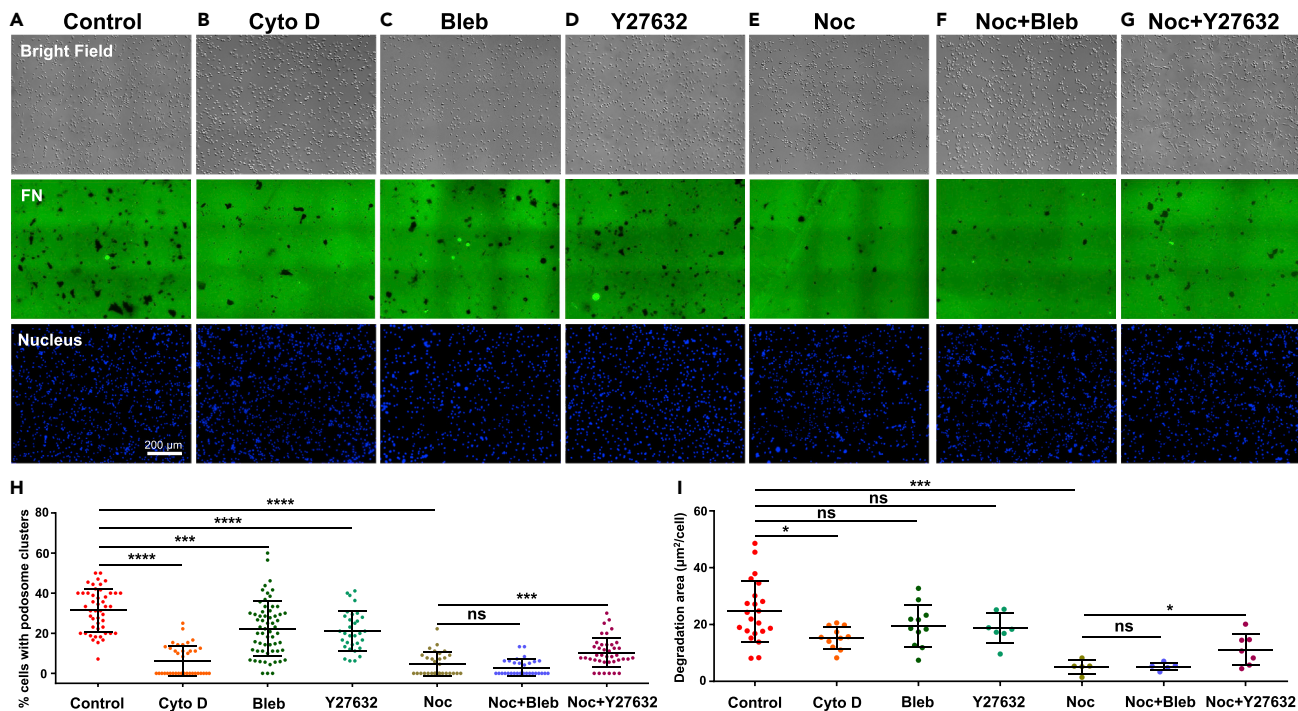
Figure 6. The regulation of matrix degradation by different drugs in macrophages

(A–G) Representative images showing the matrix degradation by macrophages cultured for 18 h together with Cyto D (100 nM), Bleb (10 μM), Y27632 (10 μM), Noc (5 μM), Noc (5 μM) + Y27632 (10 μM), and Noc (5 μM) + Bleb (10 μM). The first line shows the bright field images of macrophages. The second line shows images of fluorescence-labeled FN of the same regions. The third line shows images of cell nuclei stained by DAPI.

(H) Box chart showing a summary of the percentage of cells with podosome clusters under different treatments for 18 h in (A–G).

(I) Box chart showing a summary of the degradation area per cell under indicated treatments in (A–G). Values are reported as means ± SD from at least three independent experiments. Statistical significances were determined by unpaired Student's t test. *p < 0.05, **p < 0.01, ***p < 0.001, ****p < 0.0001, ns, not significant (p > 0.05).

of individual macrophage podosomes, as well as defined the precise spatial relationship of the F-actin core, paxillin ring, and myosin IIA ring in the podosome structure with ~20/50 nm (lateral/axial) spatial resolution. More importantly, we found that microtubule cytoskeletons directly passed through the podosomes of macrophages and regulated their assembly.

We started by showing that during *in vitro* culturing, mature podosomes tended to form higher ordered groups as podosome clusters (Figure 1B). The effective assembly of podosome structure forms the basis of matrix degradation by macrophages.[8,18,19] Grouping individual podosomes into large clusters may help enhance the matrix degradation capability. In our results, macrophages formed podosome clusters and degraded matrix in a time-dependent way (Figure 1F), and the positions of matrix degradation corresponded to where podosome clusters formed (Figure S4). Moreover, we observed that macrophages degraded the extracellular matrix in a "plaque erasing" manner (Figure S6 and Video S1), suggesting podosome clusters may exhibit strong collective movement for degrading the matrix. Therefore, the podosome cluster acts as an integral structure rather than single separate podosomes to execute the function in macrophages.

Since individual podosomes are submicron sized with various components, the delicate spatial orchestration of podosomes is difficult to study with the conventional light microscope. In recent studies, more and more researchers imaged podosomes utilizing a variety of super-resolution methods, which greatly enhanced the understanding of the podosome ultrastructure and function.[27–35] In the present work, through dual-color 3D-STORM images of individual podosomes, we clearly visualized that podosomes exhibited typical structures with "F-actin core" + "Paxillin/Myosin IIA ring" as previously described[9–11,18,30,33] (Figure 2). By learning from the particle averaging algorithms that have been used to resolve the

ultrastructure of nuclear pore complexes[47] and centrioles,[48] we developed a particle superimposing method by the alignment and combination of multiple 3D-STORM images. Our method can significantly enhance the data extraction capability to make up for the labeling density limitation of immunofluorescence, thus obtaining more precise information for the localizations and interactions of individual components in podosomes. Applying this approach, we clearly and visually sketched a snowman-like 3D portrait of podosome F-actin core surrounded by the ring-like paxillin (Figure 2I) or myosin IIA (Figure 2J). We next provided the nanoscale z-distribution profiles of the two podosome component pairs (Figures 2K and 2L). We thus determined a ~90 nm difference in the axial localization between the paxillin ring and the myosin IIA ring in macrophage podosomes, which is indistinguishable from diffraction-limited microscopy. Since the first description of podosome structure, several architectural models of podosome subdomains were continually proposed by gathering the information from data obtained in different cell types.[18,28,33,49,50] The data we presented here will help to enrich the picture of this system.

We further revealed the detailed spatial connections of podosomes to microtubules in macrophages (Figure 3). Accumulated evidence has indicated that microtubules directly or indirectly contact adhesive structures, including podosomes and focal adhesions, to regulate their dynamics and positioning.[39–43,51] Some microtubule-binding proteins, including the kinesin KIF1C, cytoplasmic linker-associated proteins, and plus-end tracking proteins like EB1, play key roles in capturing microtubule plus ends to podosomes.[40,52–55] Here, utilizing dual-color 3D-STORM imaging, we showed that in some cases microtubules passed through, rather than ended at, macrophage podosomes (Figure 3A). A possible explanation is that podosomes are highly dynamic structures with continuous oscillation. Those dynamic states may transiently allow microtubules to enter and cross the podosome core to form a mechanical link between podosomes and microtubules, and thus may provide a strong physical support for maintaining the podosome structures. The discrepancy between our results and previous studies on how microtubules interact with podosomes may be resulted from the resolution restrictions of traditional microscopy, or the using of different cell systems. For instance, in their cell systems, previous work paid more attention to the contaction of podosomes by microtubule plus ends at the cell periphery,[40,52,53] while primary peritonel macrophages predominantly form compact podosome clusters in the cell interior. Together with particle superimposing, we further validated that microtubules crossed podosomes at the level of myosin IIA (Figure 3B), suggesting a possible myosin IIA-driven linkage between podosomes and microtubules. Interestingly, in an earlier report, it was suggested that the kinesin KIF1C at microtubule plus ends could interact with podosome-localized myosin IIA, thus providing an interface for the intracellular targeting of podosomes by microtubules.[40] This finding was consistent with our notion of the involvement of myosin IIA in the connections of podosomes with microtubule cytoskeletons.

For the regulation of podosome assembly, actin polymerization is known to serve as the driving force behind most podosome characteristics.[30] Myosin IIA bundled to unbranched actin filaments that emanate radially from the F-actin cores of podosomes is also thought to be involved in regulating podosome dynamics.[56–58] Strikingly, conflicting data existed on the role of myosin IIA in podosome regulation. For instance, blocking myosin II contractility by Bleb could stimulate or enhance the formation of podosomes in N1E-115 neuroblastoma cells,[59] megakaryocytes,[60] and A7r5 vascular smooth muscle cells,[61] however inhibited the assembly of podosomes in human peripheral blood mononuclear macrophages,[40] NIH-3T3 fibroblasts,[62] and BHK-RSV cells,[20] and had little influence on the emergence of podosomes in dendritic cells.[30,56,63] In the present work, we found that the formation of podosome clusters was dependent on actin polymerization (Figures S6A and S6D) but was largely independent of myosin IIA contractility (Figure 4). Even so, inhibiting the activity of myosin IIA could influence the distribution of myosin IIA in the region of podosome clusters (Figures 4 and S8) as well as prevent the connections of microtubules to podosomes (Figure S9), and thereby may induce podosome instability and influence the assembly dynamics of podosome structures.

On the other hand, the turnover of podosomes could be regulated by a variety of intracellular signal pathways, particularly the Rho/ROCK-myosin II signaling.[63–65] As previously reported, microtubule depolymerization leads to the release of guanine nucleotide exchange factor from the microtubule lattice, which consequently activates the Rho/ROCK signaling axis.[42,43] Rho/ROCK is known to activate actomyosin contractility, which is favorable for the growth of stress fiber-associated focal adhesions but detrimental to the assembly of podosomes.[42,43] It has been reported that PGE2 stimulation leads to Rho/ROCK activation-dependent podosome loss in dendritic cells, and inhibition of Rho/ROCK axis by Y27632 or

suppression of myosin II activity downstream Rho/ROCK by Bleb blocked PGE2-elicited podosome loss.[63] As expected, when we treated macrophages with the microtubule-depolymerizing drug Noc, it led to the drastic disassembly of podosome clusters (Figure 5C). However, Y27632 or Bleb only partially abolished the Noc-induced podosome disassembly (Figure 5C). These results suggested that mechanisms other than the activation of the Rho/ROCK-myosin IIA pathway are required to explain the dissolution of podosomes upon microtubule destruction.

Notably, a recent paper reported that the loss of Golgi microtubules did not affect Rho activity but regulated the dynamics of focal adhesions.[66] Thus, microtubules may regulate the assembly of subcellular adhesive structures via different pathways. As we presented above, microtubules crossed the podosomes to provide a physical support for maintaining their structures. Thus, the microtubule interactions and Rho/ROCK-myosin IIA signal pathway may both contribute to the assembly of podosome in macrophages (Figure 5D). Noc-elicited microtubule disruption can simultaneously trigger the activation of the signal pathway and cause loss of the physical support, both of which will lead to the disassembly of podosomes (Figure 5D). Applying Bleb or Y27632 alone to the cells suppresses the Rho/ROCK signal pathway but promotes the loss of the physical support, thereby resulting in a neutralizing effect on podosome occurrence. Accordingly, we can explain why the two drugs only partially prevented the Noc-induced podosome dissolution. Interestingly, Y27632 evoked a little stronger reformation of podosomes than that of Bleb (Figure 5C); this may be due to their different inhibitory roles on myosin IIA activity. Afterward, our results showed that podosome cluster-mediated matrix degradation was also regulated by the actomyosin network and microtubule cytoskeletons, which verified that the structure of podosome clusters determined the function of matrix degradation (Figures 6 and S14).

In summary, the present work revealed that during *in vitro* cell culturing, primary mouse macrophages form high-ordered podosome clusters which initiate time-dependent extracellular matrix degradation. Based on the powerful 3D-STORM super-resolution light microscopy, we addressed the nanoscale arrangement of podosome actin core and ring components, as well as demonstrated that microtubules pass through podosomes at the level of myosin IIA. Moreover, we developed a particle superimposing method for 3D reconstruction of podosome component pairs by combining multiple images of individual podosomes, improving the visualization and analysis of z-distribution of different podosome components. Combined with pharmacological approaches, we suggested that microtubules physically stabilize podosome clusters formed in macrophages in addition to regulate their assembly through the commonly assumed Rho/ROCK-myosin IIA signaling. Our findings will enrich the information of the nanoscale architecture of podosomes, as well as provide insights in understanding the regulation of the matrix-degrading podosomes in macrophages.

Limitations of the study

In this study, 3D-STORM allows us to resolve the ultrastructural organization of individual podosomes in primary macrophages with ∼20/50 nm (lateral/axial) spatial resolution, yet owing to the technical limitation, we can only perform the imaging experiments in fixed cells. Future studies on podosome dynamics especially longitudinal dynamics within single macrophages by live cell imaging will strengthen the present study. Additionally, here, we mainly focused on the precise localization of podosome ring protein paxillin and myosin IIA; further investigations will also be required to address the arrangement of other podosome components, such as the cap protein zyxin. On the other hand, although our results indicated that microtubules pass through podosomes at the layer of myosin IIA to physically stabilize podosome clusters formed in macrophages, there is still a lack of mechanistic insights into how and why microtubules cross podosomes overcoming the steric hindrance of podosome F-actin core, and it would be interesting to determine the detailed roles of myosin IIA in driving the mechanical link between podosomes and microtubule cytoskeletons.

STAR★METHODS

Detailed methods are provided in the online version of this paper and include the following:

- KEY RESOURCES TABLE
- RESOURCE AVAILABILITY
  - Lead contact
  - Materials availability

SUPPLEMENTAL INFORMATION

Supplemental information can be found online at https://doi.org/10.1016/j.isci.2022.105514.

AUTHOR CONTRIBUTIONS

L.P. conceived the research and were in charge of overall direction. L.P. and F.H. designed the experiments. D.Z. and P.Z. performed the experiments and collected the data. F.H., D.Z., and H.D. analyzed the data and prepared the figures with the help of W.L. and R.Y. F.X. contributed to sample preparation. J.Z. and K.X. contributed to the interpretation of the results. F.H. wrote the manuscript with help of L.P. and K.X. All authors participated in discussions. L.P., K.X., and J.X. supervised the work.

DECLARATION OF INTERESTS

The authors declare no competing interests.

INCLUSION AND DIVERSITY

We support inclusive, diverse, and equitable conduct of research.

REFERENCES

1. Franken, L., Schiwon, M., and Kurts, C. (2016). Macrophages: sentinels and regulators of the immune system. Cell Microbiol. 18, 475–487.

2. den Haan, J.M.M., and Kraal, G. (2012). Innate immune functions of macrophage subpopulations in the spleen. J. Innate Immun. 4, 437–445.

3. Oishi, Y., and Manabe, I. (2018). Macrophages in inflammation, repair and regeneration. Int. Immunol. 30, 511–528.

4. Shi, C., and Pamer, E.G. (2011). Monocyte recruitment during infection and inflammation. Nat. Rev. Immunol. 11, 762–774.

5. Xuan, W., Qu, Q., Zheng, B., Xiong, S., and Fan, G.H. (2015). The chemotaxis of M1 and M2 macrophages is regulated by different chemokines. J. Leukoc. Biol. 97, 61–69.

6. Le Clainche, C., and Carlier, M.F. (2008). Regulation of actin assembly associated with protrusion and adhesion in cell migration. Physiol. Rev. 88, 489–513.

7. Webb, D.J., Parsons, J.T., and Horwitz, A.F. (2002). Adhesion assembly, disassembly and turnover in migrating cells – over and over and over again. Nat. Cell Biol. 4, E97–E100.

8. Wiesner, C., Le-Cabec, V., El Azzouzi, K., Maridonneau-Parini, I., and Linder, S. (2014). Podosomes in space: macrophage migration and matrix degradation in 2D and 3D settings. Cell Adh. Migr. 8, 179–191.

9. Evans, J.G., and Matsudaira, P. (2006). Structure and dynamics of macrophage podosomes. Eur. J. Cell Biol. 85, 145–149.

10. Van Goethem, E., Guiet, R., Balor, S., Charrière, G.M., Poincloux, R., Labrousse, A., Maridonneau-Parini, I., and Le Cabec, V. (2011). Macrophage podosomes go 3D. Eur. J. Cell Biol. 90, 224–236.

11. Murphy, D.A., and Courtneidge, S.A. (2011). The 'ins' and 'outs' of podosomes and invadopodia: characteristics, formation and function. Nat. Rev. Mol. Cell Biol. 12, 413–426.

12. Mersich, A.T., Miller, M.R., Chkourko, H., and Blystone, S.D. (2010). The formin FRL1 (FMNL1) is an essential component of macrophage podosomes. Cytoskeleton 67, 573–585.

13. Van Audenhove, I., Debeuf, N., Boucherie, C., and Gettemans, J. (2015). Fascin actin bundling controls podosome turnover and disassembly while cortactin is involved in podosome assembly by its SH3 domain in THP-1 macrophages and dendritic cells. Biochim. Biophys. Acta 1853, 940–952.

14. Panzer, L., Trübe, L., Klose, M., Joosten, B., Slotman, J., Cambi, A., and Linder, S. (2016). The formins FHOD1 and INF2 regulate inter- and intra-structural contractility of podosomes. J. Cell Sci. 129, 298–313.

15. van den Dries, K., Bolomini-Vittori, M., and Cambi, A. (2014). Spatiotemporal organization and mechanosensory function of podosomes. Cell Adh. Migr. 8, 268–272.

16. Daubon, T., Buccione, R., and Génot, E. (2011). The Aarskog-Scott syndrome protein Fgd1 regulates podosome formation and extracellular matrix remodeling in transforming growth factor beta-stimulated aortic endothelial cells. Mol. Cell Biol. 31, 4430–4441.

17. Takito, J., Inoue, S., and Nakamura, M. (2018). The sealing zone in osteoclasts: a self-organized structure on the bone. Int. J. Mol. Sci. 19, 984.

18. Linder, S., Wiesner, C., and Himmel, M. (2011). Degrading devices: invadosomes in proteolytic cell invasion. Annu. Rev. Cell Dev. Biol. 27, 185–211.

19. Van Goethem, E., Poincloux, R., Gauffre, F., Maridonneau-Parini, I., and Le Cabec, V. (2010). Matrix architecture dictates three-dimensional migration modes of human macrophages: differential involvement of proteases and podosome-like structures. J. Immunol. 184, 1049–1061.

20. Collin, O., Na, S., Chowdhury, F., Hong, M., Shin, M.E., Wang, F., and Wang, N. (2008). Self-organized podosomes are dynamic mechanosensors. Curr. Biol. 18, 1288–1294.

21. Labernadie, A., Bouissou, A., Delobelle, P., Balor, S., Voituriez, R., Proag, A., Fourquaux, I., Thibault, C., Vieu, C., Poincloux, R., et al. (2014). Protrusion force microscopy reveals oscillatory force generation and mechanosensing activity of human macrophage podosomes. Nat. Commun. 5, 5343.

22. Linder, S., Nelson, D., Weiss, M., and Aepfelbacher, M. (1999). Wiskott-Aldrich syndrome protein regulates podosomes in primary human macrophages. Proc. Natl. Acad. Sci. USA 96, 9648–9653.

23. Iqbal, Z., Cejudo-Martin, P., de Brouwer, A., van der Zwaag, B., Ruiz-Lozano, P., Scimia, M.C., Lindsey, J.D., Weinreb, R., Albrecht, B., Megarbane, A., et al. (2010). Disruption of the podosome adaptor protein TKS4 (SH3PXD2B) causes the skeletal dysplasia eye, cardiac abnormalities of Frank-Ter Haar Syndrome. Am. J. Hum. Genet. 86, 254–261.

24. Gimona, M., Buccione, R., Courtneidge, S.A., and Linder, S. (2008). Assembly and biological role of podosomes and invadopodia. Curr. Opin. Cell Biol. 20, 235–241.

25. Dovas, A., and Cox, D. (2011). Signaling networks regulating leukocyte podosome dynamics and function. Cell. Signal. 23, 1225–1234.

26. Rafiq, N.B.M., Grenci, G., Lim, C.K., Kozlov, M.M., Jones, G.E., Viasnoff, V., and Bershadsky, A.D. (2019). Forces and constraints controlling podosome assembly and disassembly. Philos. Trans. R. Soc. Lond. B Biol. Sci. 374, 20180228.

27. Cox, S., Rosten, E., Monypenny, J., Jovanovic-Talisman, T., Burnette, D.T., Lippincott-Schwartz, J., Jones, G.E., and Heintzmann, R. (2011). Bayesian localization microscopy reveals nanoscale podosome dynamics. Nat. Methods 9, 195–200.

28. van den Dries, K., Schwartz, S.L., Byars, J., Meddens, M.B.M., Bolomini-Vittori, M., Lidke, D.S., Figdor, C.G., Lidke, K.A., and Cambi, A. (2013). Dual-color super-resolution microscopy reveals nanoscale organization of mechanosensory podosomes. Mol. Biol. Cell 24, 2112–2123.

29. Walde, M., Monypenny, J., Heintzmann, R., Jones, G.E., and Cox, S. (2014). Vinculin binding angle in podosomes revealed by high resolution microscopy. PLoS One 9, e88251.

30. Meddens, M.B.M., Pandzic, E., Slotman, J.A., Guillet, D., Joosten, B., Mennens, S., Paardekooper, L.M., Houtsmuller, A.B., van den Dries, K., Wiseman, P.W., and Cambi, A. (2016). Actomyosin-dependent dynamic spatial patterns of cytoskeletal components drive mesoscale podosome organization. Nat. Commun. 7, 13127.

31. Bouissou, A., Proag, A., Bourg, N., Pingris, K., Cabriel, C., Balor, S., Mangeat, T., Thibault, C., Vieu, C., Dupuis, G., et al. (2017). Podosome force generation machinery: a local balance between protrusion at the core and traction at the ring. ACS Nano 11, 4028–4040.

32. Joosten, B., Willemse, M., Fransen, J., Cambi, A., and van den Dries, K. (2018). Super-resolution correlative light and electron microscopy (SR-CLEM) reveals novel ultrastructural insights into dendritic cell podosomes. Front. Immunol. 9, 1908.

33. van den Dries, K., Nahidiazar, L., Slotman, J.A., Meddens, M.B.M., Pandzic, E., Joosten, B., Ansems, M., Schouwstra, J., Meijer, A., Steen, R., et al. (2019). Modular actin nano-architecture enables podosome protrusion and mechanosensing. Nat. Commun. 10, 5171.

34. Foxall, E., Staszowska, A., Hirvonen, L.M., Georgouli, M., Ciccioli, M., Rimmer, A., Williams, L., Calle, Y., Sanz-Moreno, V., Cox, S., et al. (2019). PAK4 kinase activity plays a crucial role in the podosome ring of myeloid cells. Cell Rep. 29, 3385–3393.e6.

35. Hirvonen, L.M., Marsh, R.J., Jones, G.E., and Cox, S. (2020). Combined AFM and super-resolution localisation microscopy: investigating the structure and dynamics of podosomes. Eur. J. Cell Biol. 99, 151106.

36. Huang, B., Wang, W., Bates, M., and Zhuang, X. (2008). Three-dimensional super-resolution imaging by stochastic optical reconstruction microscopy. Science 319, 810–813.

37. Pan, L., Yan, R., Li, W., and Xu, K. (2018). Super-resolution microscopy reveals the native ultrastructure of the erythrocyte cytoskeleton. Cell Rep. 22, 1151–1158.

38. Pan, L., Zhang, P., Hu, F., Yan, R., He, M., Li, W., Xu, J., and Xu, K. (2019). Hypotonic stress induces fast, reversible degradation of the vimentin cytoskeleton via intracellular calcium release. Adv. Sci. 6, 1900865.

39. Linder, S., Hüfner, K., Wintergerst, U., and Aepfelbacher, M. (2000). Microtubule-dependent formation of podosomal adhesion structures in primary human macrophages. J. Cell Sci. 113, 4165–4176.

40. Kopp, P., Lammers, R., Aepfelbacher, M., Woehlke, G., Rudel, T., Machuy, N., Steffen, W., and Linder, S. (2006). The kinesin KIF1C and microtubule plus ends regulate podosome dynamics in macrophages. Mol. Biol. Cell 17, 2811–2823.

41. McMichael, B.K., Cheney, R.E., and Lee, B.S. (2010). Myosin X regulates sealing zone patterning in osteoclasts through linkage of podosomes and microtubules. J. Biol. Chem. 285, 9506–9515.

42. Rafiq, N.B.M., Nishimura, Y., Plotnikov, S.V., Thiagarajan, V., Zhang, Z., Shi, S., Natarajan, M., Viasnoff, V., Kanchanawong, P., Jones, G.E., and Bershadsky, A.D. (2019). A mechano-signalling network linking microtubules, myosin IIA filaments and integrin-based adhesions. Nat. Mater. 18, 638–649.

43. Maurin, J., Blangy, A., and Bompard, G. (2020). Regulation of invadosomes by microtubules: not only a matter of railways. Eur. J. Cell Biol. 99, 151109.

44. Schachtner, H., Calaminus, S.D.J., Thomas, S.G., and Machesky, L.M. (2013). Podosomes in adhesion, migration, mechanosensing and matrix remodeling. Cytoskeleton 70, 572–589.

45. Veillat, V., Spuul, P., Daubon, T., Egaña, I., Kramer, I., and Génot, E. (2015). Podosomes: multipurpose organelles? Int. J. Biochem. Cell Biol. 65, 52–60.

46. Faust, J.J., Balabiyev, A., Heddleston, J.M., Podolnikova, N.P., Baluch, D.P., Chew, T.L., and Ugarova, T.P. (2019). An actin-based protrusion originating from a podosome-enriched region initiates macrophage fusion. Mol. Biol. Cell 30, 2254–2267.

47. Szymborska, A., de Marco, A., Daigle, N., Cordes, V.C., Briggs, J.A.G., and Ellenberg, J. (2013). Nuclear pore scaffold structure analyzed by super-resolution microscopy and particle averaging. Science 341, 655–658.

48. Shi, X., Garcia, G., 3rd, Van De Weghe, J.C., McGorty, R., Pazour, G.J., Doherty, D., Huang, B., and Reiter, J.F. (2017). Super-resolution microscopy reveals that disruption of ciliary transition-zone architecture causes Joubert syndrome. Nat. Cell Biol. *19*, 1178–1188.

49. van den Dries, K., Linder, S., Maridonneau-Parini, I., and Poincloux, R. (2019). Probing the mechanical landscape - new insights into podosome architecture and mechanics. J. Cell Sci. *132*, jcs236828.

50. Alonso, F., Spuul, P., Daubon, T., Kramer, I., and Génot, E. (2019). Variations on the theme of podosomes: a matter of context. Biochim. Biophys. Acta. Mol. Cell Res. *1866*, 545–553.

51. Seetharaman, S., and Etienne-Manneville, S. (2019). Microtubules at focal adhesions - a double-edged sword. J. Cell Sci. *132*, jcs232843.

52. Bhuwania, R., Castro-Castro, A., and Linder, S. (2014). Microtubule acetylation regulates dynamics of KIF1C-powered vesicles and contact of microtubule plus ends with podosomes. Eur. J. Cell Biol. *93*, 424–437.

53. Efimova, N., Grimaldi, A., Bachmann, A., Frye, K., Zhu, X., Feoktistov, A., Straube, A., and Kaverina, I. (2014). Podosome-regulating kinesin KIF1C translocates to the cell periphery in a CLASP-dependent manner. J. Cell Sci. *127*, 5179–5188.

54. Biosse Duplan, M., Zalli, D., Stephens, S., Zenger, S., Neff, L., Oelkers, J.M., Lai, F.P.L., Horne, W., Rottner, K., and Baron, R. (2014). Microtubule dynamic instability controls podosome patterning in osteoclasts through EB1, cortactin, and Src. Mol. Cell Biol. *34*, 16–29.

55. Zhu, X., Efimova, N., Arnette, C., Hanks, S.K., and Kaverina, I. (2016). Podosome dynamics and location in vascular smooth muscle cells require CLASP-dependent microtubule bending. Cytoskeleton *73*, 300–315.

56. van den Dries, K., Meddens, M.B.M., de Keijzer, S., Shekhar, S., Subramaniam, V., Figdor, C.G., and Cambi, A. (2013). Interplay between myosin IIA-mediated contractility and actin network integrity orchestrates podosome composition and oscillations. Nat. Commun. *4*, 1412.

57. Bhuwania, R., Cornfine, S., Fang, Z., Krüger, M., Luna, E.J., and Linder, S. (2012). Supervillin couples myosin-dependent contractility to podosomes and enables their turnover. J. Cell Sci. *125*, 2300–2314.

58. Cervero, P., Wiesner, C., Bouissou, A., Poincloux, R., and Linder, S. (2018). Lymphocyte-specific protein 1 regulates mechanosensory oscillation of podosomes and actin isoform-based actomyosin symmetry breaking. Nat. Commun. *9*, 515.

59. Clark, K., Langeslag, M., van Leeuwen, B., Ran, L., Ryazanov, A.G., Figdor, C.G., Moolenaar, W.H., Jalink, K., and van Leeuwen, F.N. (2006). TRPM7, a novel regulator of actomyosin contractility and cell adhesion. EMBO J. *25*, 290–301.

60. Schachtner, H., Calaminus, S.D.J., Sinclair, A., Monypenny, J., Blundell, M.P., Leon, C., Holyoake, T.L., Thrasher, A.J., Michie, A.M., Vukovic, M., et al. (2013). Megakaryocytes assemble podosomes that degrade matrix and protrude through basement membrane. Blood *121*, 2542–2552.

61. Tanaka, H., Wang, H.H., Thatcher, S.E., Hagiwara, H., Takano-Ohmuro, H., and Kohama, K. (2015). Electron microscopic examination of podosomes induced by phorbol 12, 13 dibutyrate on the surface of A7r5 cells. J. Pharmacol. Sci. *128*, 78–82.

62. Collin, O., Tracqui, P., Stephanou, A., Usson, Y., Clément-Lacroix, J., and Planus, E. (2006). Spatiotemporal dynamics of actin-rich adhesion microdomains: influence of substrate flexibility. J. Cell Sci. *119*, 1914–1925.

63. van Helden, S.F.G., Oud, M.M., Joosten, B., Peterse, N., Figdor, C.G., and van Leeuwen, F.N. (2008). PGE2-mediated podosome loss in dendritic cells is dependent on actomyosin contraction downstream of the RhoA-Rho-kinase axis. J. Cell Sci. *121*, 1096–1106.

64. van Helden, S.F.G., and Hordijk, P.L. (2011). Podosome regulation by Rho GTPases in myeloid cells. Eur. J. Cell Biol. *90*, 189–197.

65. Rafiq, N.B.M., Lieu, Z.Z., Jiang, T., Yu, C.H., Matsudaira, P., Jones, G.E., and Bershadsky, A.D. (2017). Podosome assembly is controlled by the GTPase ARF1 and its nucleotide exchange factor ARNO. J. Cell Biol. *216*, 181–197.

66. Rong, Y., Yang, W., Hao, H., Wang, W., Lin, S., Shi, P., Huang, Y., Li, B., Sun, Y., Liu, Z., and Wu, C. (2021). The Golgi microtubules regulate single cell durotaxis. EMBO Rep. *22*, e51094.

67. Hu, F., Xing, F., Zhu, G., Xu, G., Li, C., Qu, J., Lee, I., and Pan, L. (2015). Rhein antagonizes P2X7 receptor in rat peritoneal macrophages. Sci. Rep. *5*, 14012.

68. Xu, K., Zhong, G., and Zhuang, X. (2013). Actin, spectrin, and associated proteins form a periodic cytoskeletal structure in axons. Science *339*, 452–456.

STAR★METHODS

KEY RESOURCES TABLE

REAGENT or RESOURCE	SOURCE	IDENTIFIER
Antibodies		
Mouse monoclonal antibodies of α-tubulin	Abcam	Cat# ab7291; RRID:AB_2241126
Rabbit monoclonal antibodies of paxillin	Abcam	Cat# ab32084; RRID:AB_779033
Purified Non-muscle Myosin Heavy Chain II-A Antibody	BioLegend	Cat# 909801; RRID:AB_2565100
Alexa Fluor 647 goat anti-mouse IgG(H+L) Highly Cross-Adsorbed Secondary Antibody	Invitrogen	Cat# A21236; RRID:AB_2535805
Alexa Fluor 647 goat anti-rabbit IgG(H+L) Highly Cross-Adsorbed Secondary Antibody	Invitrogen	Cat# A21245; RRID:AB_141775
AffiniPure Donkey Anti-Rabbit IgG (H+L)	Jackson ImmunoResearch	Cat# 711-005-152; RRID:AB_2340585
AffiniPure Donkey Anti-mouse IgG (H+L)	Jackson ImmunoResearch	Cat# 715-005-151; RRID:AB_2340759
Chemicals, peptides, and recombinant proteins		
EM-grade paraformaldehyde	Electron Microscopy Sciences	Cat# 157-8
EM-grade glutaraldehyde	Electron Microscopy Sciences	Cat# 16020
Alexa Fluor 647-conjugated phalloidin	Invitrogen	Cat# A22287
CF®568 succinimidyl ester	Biotium	Cat# 92131
DMSO	Sigma-Aldrich	Cat# D4540
Triton X-100	Sigma-Aldrich	Cat# T8787
Poly-L-lysine solution	Sigma-Aldrich	Cat# P4707
Bovine Serum Albumin (BSA)	Sigma-Aldrich	Cat# V900933
Corning® Fibronectin, Human	BD Biosciences	Cat# 354008
Hexamethyldisilazane (HMDS)	Sigma-Aldrich	Cat# 440191
Cytochalasin D	Life Technologies	Cat# PHZ1063
Blebbistatin	Sigma-Aldrich	Cat# B0506
Nocodazole	Cell Signaling Technology	Cat# 2190S
Y27632	Sigma-Aldrich	Cat# Y0503
D-(+)-Glucose	Sigma-Aldrich	Cat# G7528
Cysteamine	Sigma-Aldrich	Cat# 30070
Glucose Oxidase	Sigma-Aldrich	Cat# G2133
Catalase	Sigma-Aldrich	Cat# C30
2-(N-morpholino) ethanesulfonic acid (MES)	Sigma-Aldrich	Cat# 69892
EGTA	Sigma-Aldrich	Cat# E3889
Critical commercial assays		
CF®488A succinimidyl ester protein labeling kit	Biotium	Cat# 92213
Experimental models: Cell lines		
Primary mouse peritoneal macrophages	This paper	
Software and algorithms		
ImageJ	Open Source	http://imagej.nih.gov/
MATLAB	MathWork	http://matlab.mathworks.com
GraphPad Prism 6	GraphPad	https://www.graphpad.com/scientific-software/prism/

RESOURCE AVAILABILITY

Lead contact

Further information and requests for resources and reagents should be directed to and will be fulfilled by the lead contact, Prof. Leiting Pan (plt@nankai.edu.cn).

Materials availability

This study did not generate new unique reagents.

Data and code availability

No code is produced in this paper. All data reported in this paper will be shared by the lead contact upon request. This paper does not report original code. Any additional information required to reanalyze the data reported in this paper is available from the lead contact upon request.

EXPERIMENTAL MODEL AND SUBJECT DETAILS

Ethics statement

The animal protocol in this study conformed to the Guide for the Care and Use of Laboratory Animals (the Guide, NRC 2011), and it was also approved by the Institutional Animal Care and Use Committee at Nankai University (Approval ID 2021-SYDWLL-000072).

Macrophages isolation and culture

Healthy male C57BL/6 mice (6–8 weeks) were obtained from Beijing Vital River Laboratory Animal Technology Co., Ltd (China). C57BL/6 mice were sacrificed according to institutional guidelines. Then, Hanks' balanced salt solution (HBSS) (NaCl 150 mM, KCl 5.4 mM, $CaCl_2$ 2 mM, $MgCl_2$ 1 mM, glucose 10 mM, and HEPES 10 mM, pH = 7.4) was injected into the abdomen of each mouse. Peritoneal cells were collected from the abdomen and isolated by centrifugation at $200g$ for 10 min, which were subsequently cultured in RPMI1640 medium with 10% FBS in a humidified incubator with 5% CO_2 at 37°C. The adherent cells containing approximately 95% macrophages determined by immunostaining for Iba-1 were used in our following experiments.[67]

METHOD DETAILS

Matrix labeling and degradation

Glass coverslips were cleaned by immersion into a chromic acid lotion and then baked at 80°C for 20 min. Subsequently, they were placed for 20 min into a hermetic flask containing HMDS to enable vapor phase deposition. Fibronectin (FN) was dissolved in phosphate-buffered saline (PBS) to a concentration of 10 μg/mL and spread at room temperature for 1 h onto the prepared glass slides. To label the FN with fluorescence, the FN solution was mixed with a reactive dye (CF®488A succinimidyl ester protein labeling kit, Biotium, USA) for carrying out the labeling reaction following the instruction manual. For FN degradation assays, cells at the density of ∼1×10^5/mL were seeded on coated coverslips and incubated for indicated time courses at 37°C, followed by fixation and staining. Images were taken with an inverted fluorescence microscope (Ti-E, Nikon, Japan) equipped with a CCD camera (Retiga R1, Qimaging, Canada) using a 40×/1.3 NA oil objective. CF488A labeled FN (FN-488) was excited by a mercury lamp using a 488 nm excitation filter, and fluorescence emission was collected using a 515 nm emission filter. Matrix degradation activity was indicated by local losses of fluorescence of fibronectin. Areas of degraded matrix were then measured by ImageJ (http://imagej.nih.gov/) and expressed as degradation area per cell.

Cell fixation and immunofluorescence

Cells were seeded on 12-mm glass coverslips in a 24-well plate at ∼2×10^4 cells per well, and cultured or treated with different agents for indicated time course. For STORM imaging of actin, cells were initially fixed and extracted with a solution of 0.3% (v/v) glutaraldehyde and 0.25% (v/v) Triton X-100 in cytoskeleton buffer (CB, 10 mM MES, pH 6.1, 150 mM NaCl, 5 mM EGTA, 5 mM glucose and 5 mM $MgCl_2$) for 1 min, and then post-fixed with 2% (v/v) glutaraldehyde in CB for 15 min, a previously established protocol for maintaining the ultrastructure of actin.[68] Then, the samples were treated with freshly prepared 0.1% (w/v) sodium borohydride for 10 min to reduce background fluorescence caused by glutaraldehyde fixation. Afterward, the samples were labeled with Alexa Fluor 647 (Alexa 647) conjugated phalloidin (Invitrogen A22287) at a concentration of ∼0.4 μM for 1 h at room temperature. The samples were briefly

washed 2-3 times with phosphate buffered saline (PBS) and then immediately mounted for imaging. For imaging of other targets, the samples were fixed with 4% (w/v) paraformaldehyde in PBS for 20 min. Then, the samples were permeabilized and blocked in a blocking buffer (3% w/v BSA, 0.5% v/v Triton X-100 in PBS) for 20 min. After that, the cells were incubated with the primary antibody in the blocking buffer for 1 h at room temperature. After extensive washing in washing buffer (0.2% w/v BSA and 0.1% v/v Triton X-100 in PBS) for three times, the cells were incubated with the secondary antibody in the blocking buffer for 1 h at room temperature. Then, the samples were washed with washing buffer for three times before mounted for imaging. For two-color STORM imaging, the samples were fixed with 4% (w/v) paraformaldehyde in PBS for 20 min. Actin was labeled with Alexa647-phalloidin, the other target was immunostained with a secondary antibody conjugated with Alexa647 or CF568 succinimidyl ester. To minimize the dissociation of phalloidin from actin during washing steps, the labeling of actin was performed after all other labeling steps were completed.

3D-STORM super-resolution microscopy

After washing with PBS, the samples on the 12-mm coverslips were mounted on freshly-cleaned 22 mm × 60 mm rectangular glass slides. Briefly, 10 µL standard STORM imaging buffer containing 5% (w/v) glucose, 100 mM cysteamine, 0.8 mg/mL glucose oxidase, and 40 µg/mL catalase in Tris-HCl (pH 7.5) was dropped at the center of a rectangular glass slide, and the sample was mounted on it and subsequently sealed with Cytoseal. Then, the fluorescence images were collected via a homebuilt STORM setup based on an inverted optical microscope (Ti-E, Nikon, Japan) equipped with an EMCCD (iXon Ultra 897, Andor, UK) using an oil-immersion objective (Nikon CFI Plan Apochromat λ, 100×, numerical aperture = 1.45), as described in our previous work.[37,38] Lasers at 405, 560, and 647 nm were introduced into the cell sample through the back focal plane of the objective, and shifted towards the edge of the objective to illuminate ~1 µm within the glass-water interface. A strong (~2 kW cm^{-2}) excitation laser of 647 nm photoswitched most of the labeled dye molecules into a dark state, while also exciting fluorescence from the remaining, sparsely distributed emitting dye molecules for single-molecule localization. A weak 405-nm laser (typical range 0–1 W cm^{-2}) was used concurrently with the 647-nm or 560-nm laser to reactivate fluorophores into the emitting state, so that at any given instant, only a small, optically resolvable fraction of fluorophores was in the emitting state. A cylindrical lens was put into the imaging path to introduce astigmatism to encode the depth (z) position into the ellipticity of the single-molecule images. The EMCCD concurrently recorded images at 110 frames per second for a frame size of 256 × 256 pixels at an effective pixel size of 160 nm in the sample space, and typically recorded ~50,000 frames per image to determine the location of each molecule using the localization algorithm described previously,[36] in which the centroid positions and ellipticities of the single-molecule images obtained in each frame were respectively used to deduce the lateral and axial positions of each molecule. Thus, 3D-STORM super-resolution images were reconstructed from the single-molecule images. For each experimental condition, more than 10 cells were imaged, with representative results shown in the main and the supplementary figures.

3D-STORM image analysis

For analysis of the circularity and radius of podosomes in macrophages, a STORM image of actin was first converted to an 8-bit grayscale image by ImageJ. Then, the information of podosomes in this grayscale image was extracted by adjusting the threshold value of image to highlight the morphology of each separate podosome. After accomplishing this image identification, the circularity and radius of each podosome were measured using the "Analyze Particles" (Shape descriptors and Feret's diameter) tool of ImageJ. Hundreds of podosomes in at least 10 macrophages from three independent experiments were analyzed for each experimental condition.

Particle superimposing method

To reconstruct the 3D-portraits of different podosome component pairs (actin/paxillin, actin/myosin IIA or actin/α-tubulin), sixty individual podosomes in 10–15 dual-color STORM images of macrophages from three independent experiments were randomly selected, and the x, y, z coordinates of all signal points in each selected podosome were extracted. After that, a custom-written MATLAB routine was used to identify the center of the actin core in xy direction for each podosome (Figure S15), and then all the actin signal particles from the sixty podosomes were aligned and combined together by setting their center as the origin in x and y directions, with the z positions keeping unchanged. Simultaneously, the corresponding paxillin, myosin IIA and α-tubulin signal particles were also aligned and combined together following the recognized actin xy centers to obtain the composite 3D graphics for the three podosome component

pairs, respectively. By projection of the composite graphics in z direction and statistical analysis of the z-coordinates of all signal particles can thereby obtain the z-distribution profiles for the three podosome component pairs.

QUANTIFICATION AND STATISTICAL ANALYSIS

All data are presented as mean $\pm$ standard deviation (SD) from at least three independent experiments. The statistical comparison between the two groups was carried out using unpaired Student's t-test (GraphPad Prism 6). Statistical significance was defined as $*p < 0.05$, $**p < 0.01$, $***p < 0.001$, $****p < 0.0001$, ns, not significant ($p > 0.05$).